Delft University of Technology

Numerical study of the effect of head and eye movement on progression of retinal detachment

Vroon, J.; de Jong, J. H.; Aboulatta, A.; Eliasy, A.; van der Helm, F. C.T.; van Meurs, J. C.; Wong, D.; Elsheikh, A.

Important note
To cite this publication, please use the final published version (if applicable).
Please check the document version above.

ORIGINAL PAPER

Numerical study of the effect of head and eye movement on progression of retinal detachment

J. Vroon[1] · J. H. de Jong[2] · A. Aboulatta[3] · A. Eliasy[3] · F. C. T. van der Helm[1] · J. C. van Meurs[2,4] · D. Wong[3] ·
A. Elsheikh[3]

Abstract

Rhegmatogenous retinal detachment (RD) is a sight threatening condition. In this type of RD a break in the retina allows retrohyaloid fluid to enter the subretinal space. The prognosis concerning the patients' visual acuity is better if the RD has not progressed to the macula. The patient is given a posturing advice of bed rest and semi-supine positioning (with the RD as low as possible) to allow the utilisation of gravity and immobilisation in preventing progression of the RD. It is, however, unknown what external loads on the eye contribute the most to the progression of a RD. The goal of this exploratory study is to elucidate the role of eye movements caused by head movements and saccades on the progression of an RD. A finite element model is produced and evaluated in this study. The model is based on geometric and material properties reported in the literature. The model shows that a mild head movement and a severe eye movement produce similar traction loads on the retina. This implies that head movements—and not eye movements—are able to cause loads that can trigger and progress an RD. These preliminary results suggest that head movements have a larger effect on the progression of an RD than saccadic eye movements. This study is the first to use numerical analysis to investigate the development and progression of RD and shows promise for future work.

Keywords Finite element modelling · Numerical simulation · Retinal detachment · Saccadic eye movement · Head movement

J. Vroon, J. H. de Jong: joint principle authorship.

✉ J. Vroon
  josvroon@gmail.com

  J. H. de Jong
  H.dejong@oogziekenhuis.nl

  A. Aboulatta
  a.aboulatta@liverpool.ac.uk

  A. Eliasy
  a.mohammadvali@liverpool.ac.uk

  F. C. T. van der Helm
  F.C.T.vanderHelm@tudelft.nl

  J. C. van Meurs
  J.vanmeurs@oogziekenhuis.nl

  D. Wong
  David.Wong@liverpool.ac.uk

  A. Elsheikh
  Ahmed.Elsheikh@liverpool.ac.uk

[1] Delft University of Technology, Delft, The Netherlands

[2] Rotterdam Eye Hospital, Rotterdam, The Netherlands

[3] University of Liverpool, Liverpool, UK

[4] Erasmus MC, Rotterdam, The Netherlands

1 Introduction

Retinal detachment (RD) is a serious condition that can lead to blindness, in the affected eye, if left untreated. The most common type of retinal detachment is rhegmatogenous (Johnston 1991). Approximately 12–18 in 100,000 people per year are diagnosed with a primary rhegmatogenous RD (Put et al. 2013; Haimann et al. 1982). In this type of RD the interaction between the vitreous and the retina creates a break in the retina, allowing retrohyaloid fluid to enter the subretinal space.

The prognosis concerning the patients' visual ability is better if RD has not progressed to the macula (Salicone et al. 2006). Therefore, common management methods aim to keep the macula attached by slowing or halting the progression of the RD. Patients with an RD with an attached macula are scheduled for surgery as soon as possible. While waiting for surgery, these patients are advised to follow a posturing advice of bed rest and positioning on the side where the RD is mainly located. This posturing advice is often inconvenient and uncomfortable for the patient, and costly if combined with hospital admission.

Traction of the vitreous is likely to prevent reattachment of the retina. The properties of the vitreous might allow settling of the retina driven by gravity. As the retina is slightly denser than the surrounding liquefied vitreous and subretinal fluid, positioning and bed rest are prescribed to utilise the force of gravity. It is considered unlikely, however, that gravity will much affect intraocular fluid dynamics because the density difference between retina and vitreous is small (Su et al. 2009). It has long been theorised that bed rest reduces the loads on the retina caused by eye movements caused by head movements and saccades, therefore, halting progression and even causing regression of an RD (Algvere and Rosengren 1977; Lean et al. 1980). Recently, it was shown that bed rest and positioning will reduce the progression of RD. de Jong et al. (2017) also showed that during periods of interruption of bed rest the RD progresses. The progression of RD during these interruptions was caused by every day activities, like toilet visits and meal consumption. Therefore, we hypothesise that every day head movements, rather than saccadic eye movements, are a significant factor in the progression of an RD.

Performing clinical studies to investigate this hypothesis is likely to impose unacceptable risks to the patient: risking blindness by intentionally causing progression of a patients RD would be unethical, and therefore, a modelling study is indicated.

In the past, finite element models have been used to investigate impact damage in human eyes (Uchio et al. 1999; Stitzel et al. 2002; Rossi et al. 2011; Karimi et al. 2016a, b). These models have also proven useful when investigating RD due to impact (Hans et al. 2009; Liu et al. 2013). Finite element modelling provides a tool to investigate the human eye without ethical constraints. These previous studies investigated loads due to trauma, but the effect of every day eye and head movements on the progression of an existing RD has not yet been studied using finite element modelling. Numerical simulation will help to identify what conditions specifically promote extension of retinal detachment in patients where the most critical part of the retina, namely the macula, is still attached. The aim of this study is to produce a finite element model that accurately represents the human eye with an RD and elucidate the role of head and saccadic eye movements in the development and progression of an RD.

2 Materials and Methods

In this study we built finite element models of the eye and defined its geometry, the material properties, and two load cases, representing a saccadic eye movement and a head movement. Finally, we performed a parameter sensitivity analysis. The traction load on the retina generated by the two load cases was compared to each other. The general kinematics of the models were compared to ultrasound images obtained in vivo for human eyes (Accutome B-scan Plus, Malvern, USA, and Quantel Medical cinescan B-scan, Cournon d'Auvergne, France).

All models were run with a commercial finite elements software (ABAQUS Release 6.14-2, Dassault Systemes, Johnston, Rhode Island, USA). All models' geometry were generated with a custom made code run by a commercial programming software package (MATLAB Release 2015b, The MathWorks, Inc., Natick, Massachusetts, USA).

2.1 Geometry

First, we created a model involving the cornea, limbus, sclera, retina and vitreous with the dimensions shown in Fig. 1a. The 3D model is axisymmetric around the anterior–posterior axis (see Fig. 1a). For the purpose of simplicity, the increased thickness around the optic nerve head has not been modelled. The thickness of the retina is indicated in Fig. 1c, based on Chen et al. (2010, 2014), Liu et al. (2011) and Grover et al. (2010). The impact of tissues in the orbit surrounding the eye was assumed to be minimal during every day head and eye movements. Therefore, these structures were not implemented in the model.

The mesh was based on the configuration of diamatic domes as described by Nooshin and Tomatsuri (1995) and used previously by Elsheikh and Wang (2007). The cornea consisted of eleven rings of elements, the limbus consists of two rings and the sclera consists of 19 rings (see Fig. 2). The cornea, limbus, sclera and retina are represented by elements organised in one layer. All elements had a triangular prismatic shape (type C3D6). The vitreous filled the entire inner volume of the model and was made up of ten layers of elements. The three outermost element layers consist of 32 rings of elements (similar to cornea, limbus and sclera). The next set of three layers, towards the centre, consist of 16 rings of elements and the three inner-most layers consisted of eight rings of elements. The centre was filled with 192 tetrahedral elements to fill the remaining space. The elements were

(a)

(b)

(c)
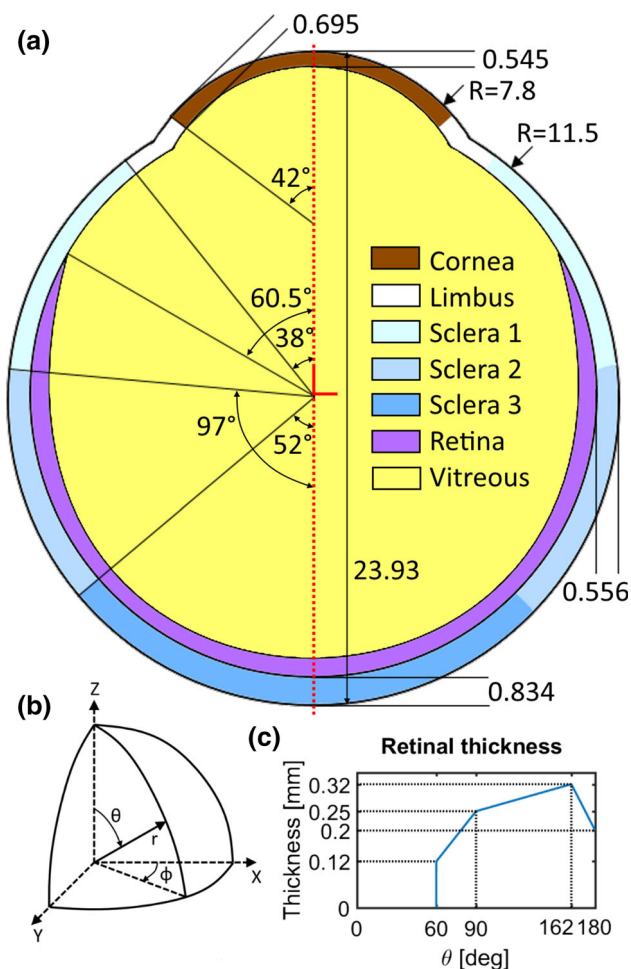
Fig. 1 **a** Schematic image (not to scale) of a cross section of the model through the *xz*-plane. All measurements are in millimetres and all angles in degrees. The colours indicate different sections of the model with different material properties (see Table 1). The red lines indicate the location of the origin of the coordinate system. The model is axisymmetric around the *z*-axis (red dotted line). **b** Direction and orientation of the Cartesian and polar coordinates used in the model. The *z*-axis runs anterior–posteriorly. **c** Graph of the thickness of the retina, as a function of θ (**b**). The graph starts at 60° because at lower θ angles the retina is not present

attached to the adjacent elements using a tie constraint. See Table 1 for an overview of all elements in the model.

We now have the model as shown in Fig. 3a. Next, the vitreous was shrunk posteriorly to create a posterior vitreous detachment. This was accomplished by transposing nodes of the vitreous inward. The amount is described with the following equations:

$$r_{\text{new}} = r * f_{\text{shrink}}(\theta) \tag{1}$$

where r is the r-coordinate of the node as described by the spherical coordinate system shown in Fig. 1b. The term $f_{\text{shrink}}(\theta)$ is described as:
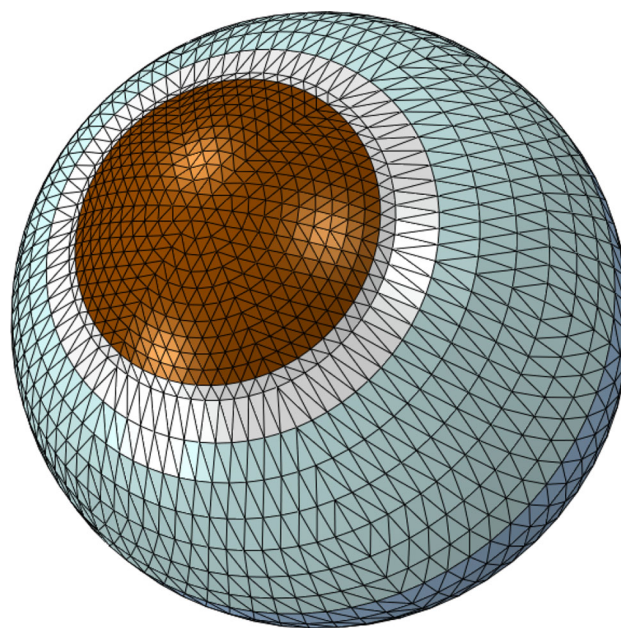
Fig. 2 A 3D rendering of the model showing the mesh layout. The mesh was based on the design for a diamatic dome as described by Nooshin and Tomatsuri (1995). The cornea (brown) plus one ring of the limbus count twelve rings of elements. The sclera (various shades of blue) plus one ring of the limbus count 20 rings, making for a total of 32 rings of elements. All elements have a triangular prism shape

$$f_{\text{shrink}}(\theta) = \begin{cases} 1 & \text{for} \quad 0 \leq \theta \leq 86° \\ -\frac{3}{8}\theta + \frac{25}{16} & \text{for} \quad 86° < \theta \leq 144° \\ \frac{1}{2\cos\pi - \theta} & \text{for} \quad 144° < \theta \leq 180° \end{cases} \tag{2}$$

where θ is the θ-coordinate as described by the polar coordinate system shown in Fig. 1b. Thus, Eq. (1) defines a new r-coordinate for all nodes of the vitreous dependent on the θ-coordinate. See Fig. 3b.

Finally, an RD was created by transposing the nodes of the retina and the nodes of the vitreous towards the centre. The transposing was done in a similar way as before (see Eq. 1) but now with an extra factor dependent on ϕ (see Fig. 1b).

$$r_{\text{new}} = r * (1 - 0.06 * f_{rd}(\theta) * f_{rd}(\phi)) \tag{3}$$

where $f_{rd}(\theta)$ is defined in Eq. (4) and $f_{rd}(\phi)$ is defined in Eq. (5).

$$f_{rd}(\theta) = \begin{cases} -10\left(\theta - \frac{29}{50}\pi\right)^2 + 4 & \text{for } 66° \leq \theta \leq 144° \\ 0 & \text{for all other } \theta \end{cases} \tag{4}$$

$$f_{rd}(\phi) = \begin{cases} -5\phi^2 + 1 & \text{for } -26° \leq \phi \leq 26° \\ 0 & \text{for all other } \phi \end{cases} \tag{5}$$

Thus, Eq. (3) gives a definition for the new r-coordinate of all nodes of the vitreous and the retina dependent on the

Table 1 Regions of the model with element types, number of elements and material properties

Region	# of elements	Density (kg/m^3)	Stiffness
Cornea	726	1061	Ogden: $n = 1$
			$\mu = 54100\,\text{Pa}$
			$\alpha = 110.4$
Limbus	288	1076	Ogden: $n = 1$
			$\mu = 270910.5\,\text{Pa}$
			$\alpha = 150$
Sclera1	1044	1076	Ogden: $n = 1$
			$\mu = 270910.5\,\text{Pa}$
			$\alpha = 150$
Sclera2	720	1076	Ogden: $n = 1$
			$\mu = 133,279\,\text{Pa}$
			$\alpha = 150$
Sclera3	294	1076	Ogden: $n = 1$
			$\mu = 133,279\,\text{Pa}$
			$\alpha = 150$
Vitreous	12,288	1005	Young's: $E = 15\,\text{Pa}$
			$\nu = 0.495$
Retina	1536	1033	Ogden: $n = 1$
			$\mu = 12021\,\text{Pa}$
			$\alpha = 145$

Material properties of the cornea, limbus and sclera were based on in house measurements performed by the University of Liverpool [most recent publication by Whitford et al. (2015)]. The properties of the vitreous were based on the average of four publications (Pokki et al. 2015; Swindle et al. 2008; Bettelheim and Wang 1976; Zimmerman 1980). The properties of the retina were based on data provided and published by Chen et al. (2014). The vitreous was modelled using a Young's modulus combined with a Poisson ratio (it is modelled as a solid). All other material stiffnesses were approximated using the Ogden material model (Ogden 1972)

θ-coordinate and the ϕ-coordinate. The transposing of the nodes finalises the model geometry (see Fig. 3c).

The previous equations, defining the vitreous detachment and the RD, have been defined in consultation with a veteran vitreoretinal surgeon (J.C.v.M) to create a realistic pathological case.

2.2 Materials

The material properties used in the model, and their sources are shown in Table 1. Due to the lack of more accurate measurements, the vitreous was modelled as a solid material with a Young's modulus and a Poisson ratio. All other materials were defined with hyperelastic Ogden material constitutive models (Ogden 1972). More accurate material models are known for the cornea, sclera and limbus that may also incorporate microstructures. These properties were not found necessary to be used in this study. These com-
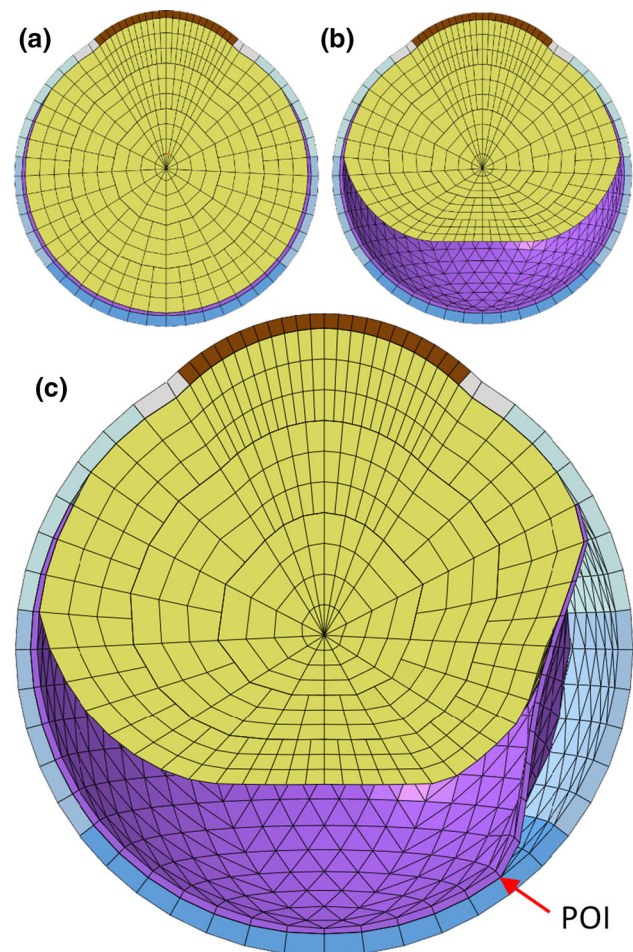
Fig. 3 The steps in building the geometry of the model. Shown is a cross section through the xz-plane (Fig. 1b). The colours correspond to the materials as seen in Fig. 1a. **a** First step in building the model, exactly like Fig. 1a. **b** Second step, the model with a detached vitreous. (see Eq. 3). **c** Final step, the model with a detached vitreous and an RD. The red arrow indicates the location of the point of interest (POI) where the results are measured

ponents are much stiffer than the vitreous and retina and therefore acting as a rigid body during every day head and eye movements. Authors believe that other components of the eye including Lens, Iris and optic nerve head will not play a significant role for the purpose of this study, and since the material characteristics of these components are not accurately known, these implementation could result in a less reliable numerical models and increases uncertainties.

The free liquefied vitreous between vitreous and retina, and in the subretinal space between retina and sclera, was modelled using the FLUID CAVITY option available in ABAQUS. The fluid cavity was characterised by an enclosing surface and a bulk modulus that describes the compressibility. The bulk modulus was set at 1 kPa to simulate (near) incompressible behaviour. This adds a constraint to the enclosed

volume of the fluid cavity of compressibility in compliance with the defined bulk modulus. The cavity will therefore act as one big element that can deform at will but must keep its volume constant.

The mass of the free fluid was added evenly to the elements surrounding a cavity using the NON STRUCTURAL MASS option. The cavities (one above and one underneath the retina) can exchange fluid with each other through a retinal break based on pressure difference, viscosity, flow area and flow coefficient. Liquefied vitreous is very similar to water in physical and mechanical properties (Godtfredsen 1949); therefore, the viscosity was set to that of water (0.001 Pa s). The flow area was set to 1 mm^2 which is a typical size for a retinal break (Miura and Ideta 2000; Neumann and Hyams 1972). The flow constant was set to 0.65; this is comparable to flow through a hole in a thin plate.

All models were solved using the explicit solver in ABAQUS. No convergence issues were observed and the average run time of the models was about two hours (Intel i7, 2.50 GHz, 16 GB RAM). A mesh study was performed to arrive at an optimum mesh density that provided stable behaviour predictions with the smallest number of elements. (see online resource 2)

2.3 Load cases

Two load cases were defined to investigate the differences between head and saccadic eye movements. These load cases were selected to be representative for an everyday head and eye movement. Saccadic eye movements are involuntary, and all saccades are similar, even between subjects. The load case used to represent eye movement was a saccadic eye movement of 10°. This is a large and fast saccade, larger than 95% of all saccades (Bahill et al. 1975). Saccades can be expressed with the following equation:

$$\alpha(t) = \frac{\alpha_0}{2}\left(1 - \cos\frac{\pi}{T}t\right) \tag{6}$$

where α is the rotation angle over time, t, in degrees, α_0 is the saccade angle in degrees, T is the duration of the saccade in seconds, and t is the time in seconds (Yarbus 1967). The duration of a saccade is related to the saccade angle with the empirical equation:

$$T = 0.021\,\alpha_0^{2/5} \tag{7}$$

Equations 6 and 7 were used to define a rotation over time that is imported into ABAQUS.

The head movement was defined as a translations with a size of 2 mm and a time span similar to that of the saccadic eye movement (0.1 s). The accelerations caused by this movement are comparable to a cough motion or sitting down on a chair (Arndt et al. 2004). The accelerations are larger than those created by walking but smaller than those created by jogging (Kavanagh et al. 2004). The head movement was defined using an equation similar to Eq. (6) for the progress over time:

$$s(t) = \frac{s_0}{2}\left(1 - \cos\frac{\pi}{T}t\right) \tag{8}$$

where s is the translation over time, s_0 is the size of the translation in millimetres, T is the duration of the movement in seconds, and t is the time in seconds.

Both these load cases consisted of the defined movements plus a second of stationary simulation. The movements were implemented at the outside nodes of the model (cornea, limbus and sclera). The saccadic eye rotation was defined as a counterclockwise rotation around the y-axis, and the head movements were defined as a translation in the negative x-direction (see Fig. 1b).

2.4 Parametric study

To investigate the dependency of the model on certain parameters and to investigate to what accuracy these parameters must be known, a parametric study was conducted with varying parameters related to the material properties as depicted in Table 2. One parameter has been changed at a time to investigate the effect on the models results.

We determined the traction load on the point of interest (POI) of the retina (see Fig. 3c) perpendicular to the sclera where traction pulling the retina and sclera apart is defined as positive. First, the results of the control set of parameters

Table 2 The parameters of the model that are varied to investigate dependency and needed accuracy

	Control	Variations			(%)
Vitreous density	1005 kg/m^3	90	95	105	110
Vitreous Young's	15 Pa	25	50	200	400
Retina density	1033 kg/m^3	90	95	105	110
Retina ogden (μ)	12021 Pa	25	50	200	400
Fluid viscosity	0.001 Pa * s	60	80	120	140
Fluid density	1000 kg/m^3	60	80	120	140
Retinal break	10^{-6} m^2	25	50	200	400

The control value is the average or most recent and reliable value found in the literature. The size of the variation is roughly based on the amount of variation seen in the literature. The vitreous density is based on Su et al. (2009), the vitreous stiffness is based on Pokki et al. (2015), Swindle et al. (2008), Bettelheim and Wang (1976) and Zimmerman (1980), the retinal density is based on Su et al. (2009), the retinal stiffness is based on Chen et al. (2014), the fluid viscosity is based on Godtfredsen (1949), the fluid density is based on Quintyn and Brasseur (2004), and the retinal break area is based on Miura and Ideta (2000) and Neumann and Hyams (1972)
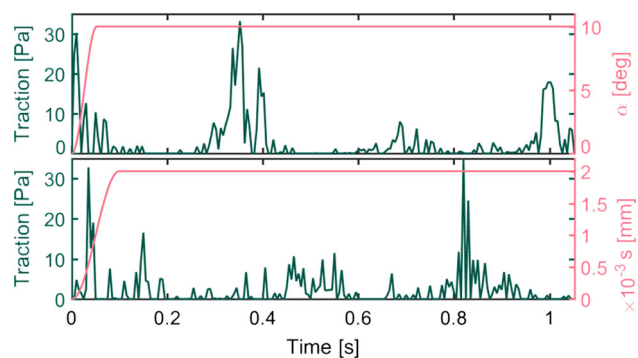
Fig. 4 Traction on the POI (see Fig. 3c) over time, for both load cases. The top graph shows the results for the eye movement (blue) and the rotation (pink) over time. The bottom graph shows the results for the head movement (blue) and the translation (pink) over time. It can be seen that in both cases oscillation of the vitreous cause traction loads on the POI long after the eye has stopped moving or rotating

were determined. The control set of parameters represent the average or best value found in the literature (see Table 2). Next, the effect of all parameter variations was determined and normalised to the loads produced by the control set of parameters. Finally, the ratio of the loads that result from the two load cases is compared for all parameter variations.

3 Results

Figure 4 shows the traction on the POI of the model with the control set of parameters for both load cases. For both load cases, the peaks in traction load are between 30 and 35 Pa. It can be seen that in both cases oscillation of the vitreous cause traction loads on the POI long after the eye has stopped moving or rotating (Fig. 5).

The results of the parametric study are shown in Fig. 6. The models result is most dependant on changes of the vitreal and retinal material properties, and also on fluid density. Note that the normalised traction load never exceeds a factor of two.

The results of the comparison between the head and saccadic eye movements are shown in Fig. 7. It shows that the ratio of the load caused by saccadic eye movements divided by the load caused by head movements is around one for most variations. Thus, head movements result in similar loads on the retina compared to saccadic eye movement.

The model has been visually compared to ultrasound images of human eyes (see online resource 1, or Fig. 5). There were clearly some differences in the shape of the vitreous bodies and the retinal detachment. Therefore, only general differences between the ultrasound recordings and the model could be observed. Two differences can be observed when comparing the model to the images. First, the vitreous in the model oscillates for a long time (also seen in Fig. 4). The ultrasound images show a single dampened movement of
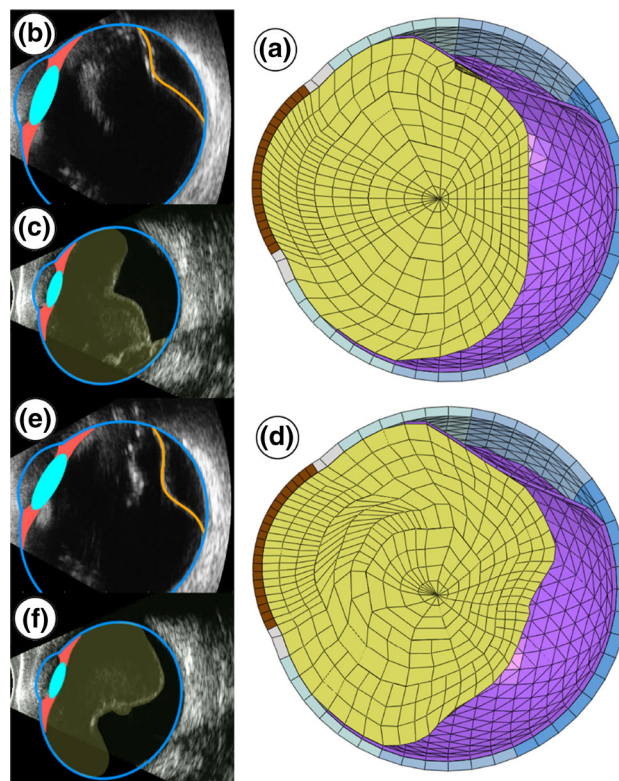
Fig. 5 Stills of the supplementary video file (online resource 1). The figure shows ultrasound imaging of two different patients: one with a retinal detachment (**b**, **e**) and one with only a vitreous detachment (**c**, **f**). Also shown is the model in similar states as the ultrasound images (**a**, **d**). The top three images **a**–**c** show the onset of eye rotation; the bottom three images **d**–**f** show the situation after rotation. The movements of the vitreous and the deformation of the retina in the ultrasound images are larger and more dampened than the movements seen in the model

the vitreous. Secondly, the ultrasound images show a more mobile retina compared to the model.

4 Conclusion and discussion

The peak of the traction loads on the retina caused by eye movements caused by head movements and saccades (Fig. 4) is within the range 30–35 Pa. Figure 6 shows that, for both load cases and all parameter variations, the traction will never change by a factor of more than two outside this 30–35 Pa range. This is a factor of ten lower than what is measured to be the adhesion force of the retina by Liu et al. (2013) which was 340 Pa. Since the defined saccadic eye movement was larger than 95% of all saccadic eye movements (Bahill et al. 1975), it is unlikely that traction caused by most saccadic eye movement will be large enough to overcome the retinal adhesion. However, the defined head movement was small compared to those created by other every day activities. Therefore, it is likely that only head movements are able to
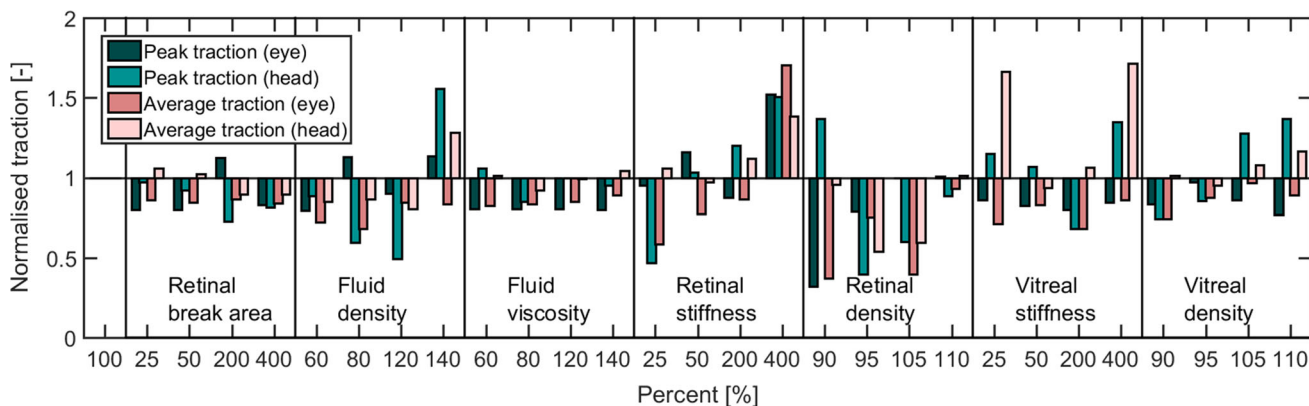
Fig. 6 Peak and average traction loads on the point of interest (normalised to the load present in the simulation with the control set of parameters) are shown on the *y*-axis. All variations of parameters are shown in the *x*-axis. The model is most sensitive for changes of the vitreal and retinal material properties
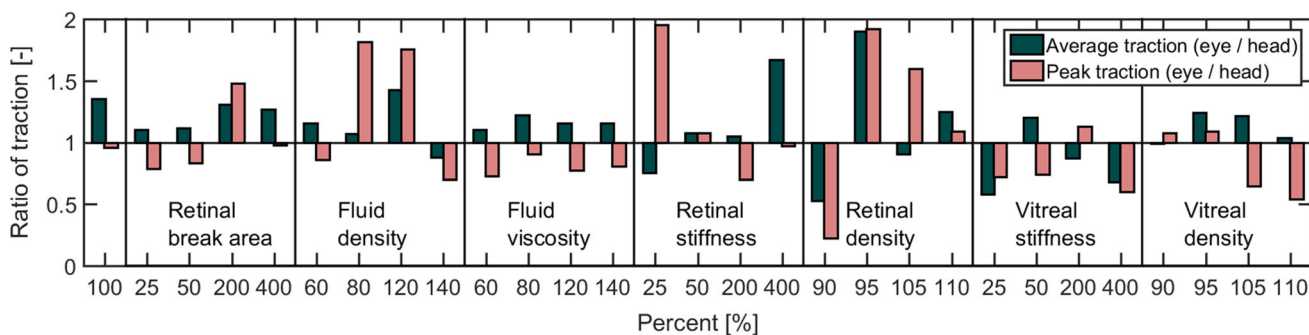
Fig. 7 The load of the rotation (eye movement) divided by the load of the translation (head movement) for all parameter variations. The ratio is shown in the *y*-axis, and the variations are shown in the *x*-axis. It can be seen that the ratio is around one for most variations. This shows that the translation (head movement) results in similar loads on the retina compared to the rotation (eye movement)

create traction loads in the same order of magnitude as the retinal adhesion. These preliminary results suggest that head movements are the major factor in the progression of an RD.

Although the ultrasound images display a simplified 2d representation of the retinal detachment, they enabled a rough comparison with the numerical model. Two observations were made when comparing the model to the ultrasound images. First, the vitreous in the model oscillates for a long period, while the real vitreous does not. This lack of damping is most likely caused by the simplifications adopted in the material properties of the vitreous and the fluid-structure interaction between vitreous and liquefied vitreous. Second, the ultrasound images show a more mobile retina compared to the model. The stiffness properties used for the retina are based on the best measurements from the literature (Chen et al. 2014). It is clear that these material properties have not been measured in a way that is physiologically representative. Only the linear material properties of the vitreous were implemented in the model, due to a lack of proper characterisation of the nonlinear and viscoelastic material properties of the vitreous in the literature. Future work is therefore needed

to measure the properties of the vitreous and retina more accurately. A better comparison to ultrasound images should also be done since there is (although small) a difference in size of the detachment between the used ultrasound images and the model.

The results of the parametric study (Fig. 6) show that the models result is most sensitive to changes of the properties of the vitreous and retina. This adds to the claim that these properties should be measured more accurately to improve the model. It should also be noted that the stiffness properties of the retina and the vitreous are known to be anisotropic and inhomogeneous (Chen et al. 2010; Chen and Weiland 2010; Colter et al. 2015). The model is less sensitive to changes of the other tissue properties. The model also shows a dependency on the densities of the liquefied vitreous, the retina and the vitreous. However, density measurements are comparatively easy and accurate. The densities are known to a greater accuracy than the stiffness (Su et al. 2009); therefore, the focus should be on measuring the stiffnesses.

This study has focused on the load produced by eye movements caused by head movements and saccades. Therefore,

gravity has been taken out of the analysis. This allowed us to purely consider the stresses produced by eye movements. Future work should aim to include gravity forces to improve the simulation. Although a realistic case was chosen in this study, it would be interesting to investigate the different presentations of the vitreous and retinal detachments and their influence on RD progression.

This study has been exploratory in nature to investigate internal eye dynamics, and it yields useful results on elucidating the role of head and saccadic eye movements in the development and progression of RD. It is the first time a finite element model has been used to investigate the pathology of an RD. The most accurate and most recent material data have been used in this model. Its preliminary results indicate that head movements are the major factor in the progression of an RD. This result could explain the results of an earlier study on the effectiveness of the posturing advice (de Jong et al. 2017). This suggests to the authors of the present paper that this modelling technique is useful in understanding the progression of RD. The fact that a relatively simple model like this produces worthwhile results shows the authors that continuation of this research will lead to better understanding of RD and could improve its treatment to minimise the risk of blindness for patients.

Compliance with ethical standards

References

Algvere P, Rosengren B (1977) Immobilization of the eye. Evaluation of a new method in retinal detachment surgery. Acta Ophthalmol 55(2):303–16

Arndt SR, Cargill II RS, Hammoud S (2004) Head acceleration experienced during everyday activities and while riding roller coasters. In: Human factors, pp 1973–1977

Bahill AT, Adler D, Stark L (1975) Most naturally occurring human saccades have magnitudes of 15 degrees or less. Investig Ophthalmol 14(June):468–469

Bettelheim FA, Wang TJY (1976) Dynamic viscoelastic properties of bovine vitreous. Exp Eye Res 23(4):435–441. https://doi.org/10.1016/0014-4835(76)90172-X

Chen K, Weiland JD (2010) Anisotropic and inhomogeneous mechanical characteristics of the retina. J Biomech 43(7):1417–1421. https://doi.org/10.1016/j.jbiomech.2009.09.056

Chen K, Rowley AP, Weiland JD (2010) Elastic properties of porcine ocular posterior soft tissues. J Biomed Mater Res Part A 93(2):635–645. https://doi.org/10.1002/jbm.a.32571

Chen K, Rowley AP, Weiland JD, Humayun MS (2014) Elastic properties of human posterior eye. J Biomed Mater Res Part A 102(6):2001–2007. https://doi.org/10.1002/jbm.a.34858

Colter J, Williams A, Moran P, Coats B (2015) Age-related changes in dynamic moduli of ovine vitreous. J Mech Behav Biomed Mater 41:315–324. https://doi.org/10.1016/j.jmbbm.2014.09.004

de Jong JH, Vigueras-Guillén JP, Simon TC, Timman R, Peto T, Vermeer KA, van Meurs JC (2017) Preoperative posturing of patients with macula-on retinal detachment reduces progression toward the fovea. Ophthalmology 124:1–13. https://doi.org/10.1016/j.ophtha.2017.04.004

Elsheikh A, Wang D (2007) Numerical modelling of corneal biomechanical behaviour. Comput Methods Biomech Biomed Eng 10(2):85–95. https://doi.org/10.1080/10255840600976013

Godtfredsen E (1949) Investigations into hyaluronic acid and hyaluronidase in the subretinal fluid in retinal detachment, partially due to ruptures and partly secondary to malignant choroidal melanoma. Br J Ophthalmol 33(12):721–732

Grover S, Murthy RK, Brar VS, Chalam KV (2010) Normative data for macular thickness by high-definition spectral-domain optical coherence tomography (spectralis). Invest Ophthalmol Vis Sci 148(2):2644–2647. https://doi.org/10.1167/iovs.09-4774

Haimann MH, Burton TC, Brown CK (1982) Epidemiology of retinal detachment. Arch Ophthalmol 100(2):289–292. https://doi.org/10.1001/archopht.1982.01030030291012

Hans SA, Bawab SY, Woodhouse ML (2009) A finite element infant eye model to investigate retinal forces in shaken baby syndrome. Graefe's Archive Clin Exp Ophthalmol 247(4):561–571. https://doi.org/10.1007/s00417-008-0994-1

Johnston PB (1991) Traumatic retinal detachment. Br J Opthalmol 75:18–21

Karimi A, Razaghi R, Navidbakhsh M, Sera T, Kudo S (2016a) Computing the stresses and deformations of the human eye components due to a high explosive detonation using fluid-structure interaction model. Injury 47(5):1–9. https://doi.org/10.1016/j.injury.2016.01.030

Karimi A, Razaghi R, Navidbakhsh M, Sera T, Kudo S (2016b) Quantifying the injury of the human eye components due to tennis ball impact using a computational fluid-structure interaction model. Injury 19(2):1–9. https://doi.org/10.1016/j.injury.2016.01.030

Kavanagh JJ, Barrett RS, Morrison S (2004) Upper body accelerations during walking in healthy young and elderly men. Gait Posture 20(3):291–298. https://doi.org/10.1016/j.gaitpost.2003.10.004

Lean JS, Mahmood M, Manna R, Chignell AH (1980) Effect of preoperative posture and binocular occlusion on retinal detachment. Br J Ophthalmol 64(2):94–97

Liu T, Hu AY, Kaines A, Yu F, Schwartz SD, Hubschman JP (2011) A pilot study of normative data for macular thickness and volume measurements using cirrus high-definition optical coherence tomography. Retina 31(9):1944–1950. https://doi.org/10.1097/IAE.0b013e31820d3f13

Liu X, Wang L, Wang C, Sun G, Liu S, Fan Y (2013) Mechanism of traumatic retinal detachment in blunt impact: a finite element study. J Biomech 46(7):1321–1327. https://doi.org/10.1016/j.jbiomech.2013.02.006

Miura M, Ideta H (2000) Factors related to subretinal proliferation in patients with primary rhegmatogenous retinal detachment. J Retin Vitreous Dis 20(5):465–468

Neumann E, Hyams S (1972) Conservative management of retinal breaks. A follow-up study of subsequent retinal detachment. Br J Ophthalmol 56(6):482–6. https://doi.org/10.1136/bjo.56.6.482

Nooshin H, Tomatsuri H (1995) Diamatic transformations. In: Giuliani C (ed) Proceedings of the symposium on spatial structures: heritage, present and future, Milan, pp 71–82

Ogden RW (1972) Large deformation isotropic elasticity–on the correlation of theory and experiment for incompressible rubberlike

solids. Proc R Soc A Math Phys Eng Sci 326(1567):565–584. https://doi.org/10.1098/rspa.1972.0026 arXiv:1205.0516v2

Pokki J, Ergeneman O, Sevim S, Enzmann V, Torun H, Nelson BJ (2015) Measuring localized viscoelasticity of the vitreous body using intraocular microprobes. Biomed Microdevices 17(5):85. https://doi.org/10.1007/s10544-015-9988-z

Quintyn JC, Brasseur G (2004) Subretinal fluid in primary rhegmatogenous retinal detachment: physiopathology and composition. Surv Ophthalmol 49(1):96–108. https://doi.org/10.1016/j.survophthal.2003.10.003

Rossi T, Boccassini B, Esposito L, Iossa M, Ruggiero A, Tamburrelli C, Bonora N (2011) The pathogenesis of retinal damage in blunt eye trauma: finite element modeling. Invest Ophthalmol Vis Sci 52(7):3994–4002. https://doi.org/10.1167/iovs.10-6477

Salicone A, Smiddy WE, Venkatraman A, Feuer W (2006) Visual recovery after scleral buckling procedure for retinal detachment. Ophthalmology 113(10):1734–1742. https://doi.org/10.1016/j.ophtha.2006.03.064

Stitzel JD, Duma SM, Cormier JM, Herring IP (2002) A nonlinear finite element model of the eye with experimental validation for the prediction of globe rupture. Stapp Car Crash J 46:81–102

Su X, Vesco C, Fleming J, Choh V (2009) Density of ocular components of the bovine eye. Optom Vis Sci 86(10):1187–95. https://doi.org/10.1097/OPX.0b013e3181baaf4e

Swindle KE, Hamilton PD, Ravi N (2008) In situ formation of hydrogels as vitreous substitutes: viscoelastic comparison to porcine vitreous. J Biomed Mater Res Part A 87(3):656–665. https://doi.org/10.1002/jbm.a.31769

Uchio E, Ohno S, Kudoh J, Aoki K, Kisielewicz LT (1999) Simulation model of an eyeball based on finite element analysis on a supercomputer. J Opthalmol 83:1106–1111

Van De Put MAJ, Hooymans JMM, Los LI (2013) The incidence of rhegmatogenous retinal detachment in the Netherlands. Ophthalmology 120(3):616–622. https://doi.org/10.1016/j.ophtha.2012.09.001

Whitford C, Studer H, Boote C, Meek KM, Elsheikh A (2015) Biomechanical model of the human cornea: considering shear stiffness and regional variation of collagen anisotropy and density. J Mech Behav Biomed Mater 42:76–87. https://doi.org/10.1016/j.jmbbm.2014.11.006

Yarbus AL (1967) Eye movements and vision. In: Haigh B, Riggs LA, Ballou LH (eds) Eye movements and vision. Plenum Press, New York, pp 129–146 (Chap IV Saccadi)

Zimmerman RL (1980) In vivo measurements of the viscoelasticity of the human vitreous humor. Biophys J 29(3):539–44. https://doi.org/10.1016/S0006-3495(80)85152-6